J. Fluid Mech. (1979), *vol.* 90, *part* 4, *pp.* 685–711
Printed in Great Britain

A hydrodynamic analysis of flagellar propulsion

By J. J. L. HIGDON

Department of Applied Mathematics and Theoretical Physics,
University of Cambridge †

(Received 1 February 1978)

The swimming of a micro-organism by flagellar propulsion is examined. The organism consists of a spherical cell body (radius A) propelled by waves travelling down a long slender flagellum (radius a, length L). Slender-body theory for Stokes flow is used to replace the flagellum with distributions of Stokeslets and dipoles along its centre-line. The cell body is represented by a Stokeslet, dipole and rotlet for translation and rotation, and by an image system to cancel the velocity induced by the singularities along the flagellum. The error in the slender-body theory is $O(a/L)$, while the images cancel the velocity on the surface of the sphere exactly. With these approximations, the boundary-value problem for the Stokes equations is transformed into a system of singular integral equations. The unknowns are the velocity and angular velocity of the organism and the force distribution along the flagellum. An iteration procedure is used to solve the equations numerically.

Numerical results are presented for planar sinusoidal waves (amplitude α, wave-number k). The average swimming speed and power consumption are computed for a wide range of the parameters. The optimal sine wave for minimizing power consumption is found to be a single wave with amplitude $\alpha k \approx 1$. The power consumption is found to be relatively insensitive to changes in the flagellar radius. The optimal flagellar length is found to be in the range $L/A = 20$–40. The instantaneous force distribution and flow field for a typical organism are presented. The trajectory of the organism through one cycle shows that a wave of constant amplitude may have the appearance of increasing amplitude owing to the yawing motion of the organism.

The results are compared with those obtained using resistance coefficients. For organisms with small cell bodies ($A/L = 0{\cdot}05$), the average swimming speed predicted by Gray–Hancock coefficients is accurate to within 10 %. For large cell bodies ($A/L = 0{\cdot}2$), the error in swimming speed is approximately 20 %. The relative error in the predicted power consumption is 25–50 %. For the coefficients suggested by Lighthill, the power is consistently underestimated. The Gray–Hancock coefficients underestimate the power for small cell bodies and overestimate it for large cell bodies.

1. Introduction

The propulsion of micro-organisms by flagellar motions is a subject with considerable interest for fluid dynamicists. The study was initiated by Taylor (1952), whose analysis gave order-of-magnitude results. Hancock (1953) presented a sophisticated model of the flagellum using line distributions of Stokeslets and potential dipoles; however, he

† Present address: Department of Chemical Engineering, Stanford University, Stanford, California 94305.

0022-1120/79/4101-0000 $00.00

was able to calculate only a few special cases owing to the complexity of the calculations. Gray & Hancock (1955) adopted a simpler model based on resistance coefficients taken from Hancock's (1953) asymptotic results. With this model, they examined the swimming of sea-urchin spermatozoa and found good agreement between the calculated and observed swimming speed. After this success, the resistance-coefficient model was adopted by all workers in the field. Brokaw (1965) used this technique to examine the locomotion of several organisms employing wave motions more general than the sinusoidal waves considered up to that point. Chwang & Wu (1971) considered helical waves and introduced the concept of moment coefficients to account for the moment generated along the flagellum. Silvester & Holwill (1972) studied a variety of biological wave forms, including very large amplitude waves which had not been studied previously. Coakley & Holwill (1972) considered a number of general three-dimensional waves, including asymmetric waves.

While the resistance-coefficient model was being applied to a variety of organisms, other researchers were examining the validity of the approach. Batchelor (1970), Cox (1970) and others refined slender-body theory through the use of perturbation methods. They gave more general results and improved values for the resistance coefficients. The weakness of their method is that it depends on an expansion in powers of $\ln \epsilon$, where ϵ is the slenderness ratio. This series requires several terms for reasonable accuracy, making it awkward to use with the complicated geometry of flagellar motions. Lighthill (1976) suggested a different formulation of slender-body theory making it convenient to find solutions $O(\epsilon)$. He suggested values for the resistance coefficients different from those of Gray & Hancock and in a certain sense 'optimal'. Johnson (1977) has developed a model of flagellar propulsion similar to that suggested by Lighthill.

In previous studies of micro-organism swimming, much attention has been given to the representation of the flagellum, but relatively little to that of the cell body. At best, the cell body has been modelled as a simple Stokeslet, dipole and rotlet with the strengths of these singularities given by Stokes' drag formula of Faxén's law. Although Faxén's law (see Happel & Brenner 1965) gives an accurate value for the force and moment on the sphere, the simple singularities do not accurately represent the flow field. Thus the Stokeslet distribution in the vicinity of the sphere may differ greatly from its actual value. The solution to this difficulty is to employ the image system for a Stokeslet in the presence of a sphere. This technique was used by de Mestre & Katz (1974) to assess the effect of the cell body on the flow around the flagellum; however, they restricted their model to the axisymmetric flow about a rigid organism moving along a line parallel to its straight flagellum. To assess properly the effect of the cell body, it is necessary to employ the complete image system as given by Oseen (1927).

In this paper, we consider organisms which are propelled by planar waves propagating down a long slender flagellum. The organism consists of a single flagellum of radius a and length L attached radially to a spherical cell body of radius A. The organisms to which this model apply are in the range $L = 10$–$10^3\,\mu$m and $a = 0{\cdot}1$–$0{\cdot}5\,\mu$m. In the case where the cell body is absent, the model applies to a variety of swimming worms with $L = 10^3\,\mu$m and $a = 10\,\mu$m. The flow is governed by Stokes' equations with the Reynolds number in the range 10^{-3}–10^{-1}. We assume that $a \ll L$ and $a \ll A$.

To find a solution to the equations, we employ distributions of the fundamental singularity and its derivatives. This reduces the problem to satisfying the no-slip

condition on the surface of the organism. Slender-body theory allows us to satisfy the boundary condition on the flagellum by a distribution of Stokeslets and dipoles along its centre-line. The error is of order a/L if the flagellum is straight, or of order $a\kappa$ if it has curvature κ. The boundary condition on the sphere is satisfied by two sets of singularities. The first set consists of image singularities which cancel the velocity on the sphere induced by the Stokeslets along the flagellum. The second set is composed of the Stokeslet, dipole and rotlet which match the velocity due to the translation and rotation of the sphere. This set of singularities is sufficient to satisfy the boundary conditions to order a/L over the entire surface of the organism.

The introduction of flow singularities transforms the no-slip boundary condition into a system of singular integral equations for the singularity distributions. These equations are too difficult to solve analytically, and the singular kernel makes it impossible to use a direct numerical solution. To circumvent this difficulty, a mixed analytical–numerical approach is used. The kernel is evaluated analytically over short intervals and the results are used to set up a system of linear algebraic equations. The diagonal of the matrix is dominant, facilitating an iterative solution.

2. Image system

The fundamental singularity of Stokes flow is called a Stokeslet and is defined by

$$S_{jk}(\mathbf{x}, \mathbf{X}) = \frac{\delta_{jk}}{r} + \frac{(x_j - X_j)(x_k - X_k)}{r^3}, \tag{1}$$

where $r = |\mathbf{x} - \mathbf{X}|$. The velocity at $\mathbf{x}$ due to a Stokeslet of strength $\mathbf{f}$ at $\mathbf{X}$ is

$$u_j(\mathbf{x}) = S_{jk}(\mathbf{x}, \mathbf{X}) f_k / 8\pi\mu. \tag{2}$$

Physically, this represents the velocity field of a point force $\mathbf{f}$ in an unbounded fluid. Mathematically, the Stokeslet is the free-space Green's function for Stokes' equations. From the theory of Green's functions, we conclude that the flow about a collection of finite bodies may be represented by distributions of Stokeslets and their normal derivatives over the body surfaces. As the Stokes equations are linear, derivatives of the Stokeslet to any order are also solutions of the equations. The first derivative is called a Stokes-doublet, the second a Stokes-quadrupole, etc. Thus, using this terminology, we state that the flow may be represented by distributions of Stokeslets and Stokes-doublets on the body surfaces. An important special case is a system of rigid bodies fixed with respect to each other, in which case the flow may be represented by distributions of Stokeslets only.

In principle, the Green's function approach provides a method for solving any problem in Stokes flow; however, in practice the difficulty in finding the required surface distributions is insurmountable. In some cases with special geometry, it is possible to circumvent this difficulty by employing the Green's function applicable to that geometry. This Green's function will consist of the Stokeslet plus a collection of image singularities which serve to cancel the velocity of the Stokeslet on the boundaries. The Green's function satisfies the no-slip condition on these boundaries implicitly, thus dispensing with singularity distributions on the surfaces considered.

Thus, in the present problem there are two ways to model the spherical cell body. The first is to consider a distribution of Stokeslets over its surface and solve the integral

equation arising from the boundary condition. This greatly complicates the solution of the problem because of the difficulty of solving an integral equation in two independent variables. The second method is to use the Green's function for the flow external to a sphere. This satisfies the boundary condition implicitly and does not introduce any new unknowns.

Oseen (1927, p. 108) gives the Green's function for the flow external to a sphere located at the origin as

$$G_{jk}(\mathbf{x},\mathbf{X}) = \frac{\delta_{jk}}{r} + \frac{(x_j - X_j)(x_k - X_k)}{r^3} - \frac{A}{|\mathbf{X}|}\frac{\delta_{jk}}{r^*} - \frac{A^3}{|\mathbf{X}|^3}\frac{(x_j - X_j^*)(x_k - X_k^*)}{r^{*3}}$$
$$- \frac{|\mathbf{X}|^2 - A^2}{|\mathbf{X}|}\left\{\frac{X_j^* X_k^*}{A^3 r^*} - \frac{A}{|\mathbf{X}|^2 r^{*3}}[X_j^*(x_k - X_k^*) + X_k^*(x_j - X_j^*)]\right.$$
$$\left. + \frac{2X_j^* X_k^*}{A^3}\frac{X_l^*(x_l - X_l^*)}{r^{*3}}\right\} - (|\mathbf{x}|^2 - A^2)\frac{\partial \phi_k}{\partial x_j} \quad (3)$$

with

$$\frac{\partial \phi_k}{\partial x_j} = \frac{|\mathbf{X}|^2 - A^2}{2|\mathbf{X}|^3}\left\{\frac{-3X_k(x_j - X_j^*)}{Ar^{*3}} + \frac{A\delta_{jk}}{r^{*3}} - \frac{3A(x_j - X_j^*)(x_k - X_k^*)}{r^{*5}}\right.$$
$$- \frac{2X_k X_j^*}{Ar^{*3}} + \frac{6X_k}{Ar^{*5}}(x_j - X_j^*)(x_l - X_l^*)X_l^* + \frac{3A}{|\mathbf{X}^*|}$$
$$\times \frac{X_k^*(x_j - X_j^*)r^{*2} + (x_j - X_j^*)(x_k - X_k^*)|\mathbf{X}^*|^2 + (r^* - |\mathbf{X}^*|)r^{*2}|\mathbf{X}^*|\delta_{jk}}{r^{*3}|\mathbf{X}^*|(|\mathbf{X}^*|r^* + x_l X_l^* - |\mathbf{X}^*|^2)}$$
$$- \frac{3A}{|\mathbf{X}^*|}\frac{(|\mathbf{X}^*|(x_j - X_j^*) + r^* X_j^*)(X_k^* r^{*2} - (x_k - X_k^*)|\mathbf{X}^*|^2 + (x_k - 2X_k^*)r^*|\mathbf{X}^*|)}{r^{*2}|\mathbf{X}^*|(|\mathbf{X}^*|r^* + x_l X_l^* - |\mathbf{X}^*|^2)^2}$$
$$\left. - \frac{3A}{|\mathbf{X}^*|}\frac{x_j X_k^* + |\mathbf{x}||\mathbf{X}^*|\delta_{jk}}{|\mathbf{x}||\mathbf{X}^*|(|\mathbf{x}||\mathbf{X}^*| + x_l X_l^*)} + \frac{3A}{|\mathbf{X}^*|}\frac{(|\mathbf{X}^*|x_j + |\mathbf{x}|X_j^*)(|\mathbf{X}^*|x_k + |\mathbf{x}|X_k^*)}{|\mathbf{x}||\mathbf{X}^*|(|\mathbf{x}||\mathbf{X}^*| + x_l X_l^*)^2}\right\}, \quad (4)$$

where A is the radius of the sphere, $\mathbf{X}^*$ is the inverse point defined by

$$\mathbf{X}^* = \frac{A^2}{|\mathbf{X}|^2}\mathbf{X} \quad (5)$$

and $r^* = |\mathbf{x} - \mathbf{X}^*|$. Therefore the velocity due to a Stokeslet of strength $\mathbf{f}$ at the point $\mathbf{X}$ in the presence of the sphere is

$$u_j(\mathbf{x}) = G_{jk}(\mathbf{x},\mathbf{X})f_k/8\pi\mu. \quad (6)$$

The expression for G_{jk} is quite complicated, but can be more easily understood if we examine its components. The first two terms are easily recognized as the Stokeslet (1). The remaining terms are the images inside the sphere. For the radial component of the Stokeslet, these can be resolved into a Stokeslet, dipole and stresslet at the inverse point $\mathbf{X}^*$. For the transverse component, they represent a line distribution of Stokelets, dipoles and Stokes-doublets extending from the origin to the inverse point.

The total Stokeslet and rotlet strengths are important as they give the force and moment on the sphere. (A rotlet is an antisymmetric Stokes-doublet and represents a point torque.) The force and moment for the radial component are

$$\mathbf{F} = \left(-\frac{3}{2}\frac{A}{|\mathbf{X}|} + \frac{1}{2}\frac{A^3}{|\mathbf{X}|^3}\right)\mathbf{f}_r, \quad \mathbf{M} = 0, \quad (7)$$

while those for the transverse component are

$$\mathbf{F} = \left(-\frac{3}{4}\frac{A}{|\mathbf{X}|} - \frac{1}{4}\frac{A^3}{|\mathbf{X}|^3}\right)\mathbf{f}_t, \quad \mathbf{M} = -\frac{A^3}{|\mathbf{X}|^3}\mathbf{X}\times\mathbf{f}_t. \tag{8}$$

As stated previously, these are in agreement with the result obtained from Faxén's law.

3. Slender-body theory

In the preceding section, we noted that the boundary condition on the organism could be satisfied by employing surface distributions of singularities. In this section, we shall show that the singularities on the surface of the flagellum can be replaced by distributions of singularities along its centre-line. This simplification is achieved through the use of slender-body theory for Stokes flow. This subject has been extensively developed in other sources (Batchelor 1970, etc.) and will not be discussed in any detail here. It will be sufficient to show that the line distributions satisfy the boundary conditions to the desired accuracy.

To satisfy the no-slip condition on the surface of the flagellum, we require that the induced velocity should match the velocity of the flagellum with respect to the fluid. At any point along the flagellum, this velocity may be viewed as that due to the translation and rotation of the cross-section at that position. We find that the translational velocity can be matched by Stokeslets and dipoles, while the rotational velocity can be matched by rotlets. We shall see that the rotational velocity is negligible for the organisms considered here. Thus the flagellum can be represented by Stokeslets and dipoles.

To show that Stokeslets and dipoles can match the translational velocity at each cross-section, we need to show that the induced velocity is approximately constant around the cross-section. From this, we infer that when the boundary condition is satisfied at all points on the centre-line it is satisfied at all points on the surface.

The dipole is defined by

$$D_{jk}(\mathbf{x},\mathbf{X}) = -\frac{\delta_{jk}}{r^3} + \frac{3(x_j - X_j)(x_k - X_k)}{r^5} \tag{9}$$

and the velocity field due to a dipole of strength $\mathbf{d}$ is

$$u_j(\mathbf{x}) = (d_k/4\pi) D_{jk}(\mathbf{x},\mathbf{X}). \tag{10}$$

In applying slender-body theory, we find that the dipole strength is determined by the Stokeslet strength and is given by

$$\mathbf{d} = (-a^2/4\mu)\mathbf{f}_\perp, \tag{11}$$

where $\mathbf{f}_\perp$ is the component of $\mathbf{f}$ in the plane perpendicular to the centre-line and a is the radius of the flagellum.

To find the velocity induced by these singularities, we consider a small section of the flagellum of length $2\delta s$. Choose a local co-ordinate system (X^L, Y^L, Z^L) with the origin at the centre of the interval and the X^L axis tangential to the centre-line. With this choice of axes, the velocity at the point $\mathbf{x}^L$ due to the singularities in the interval is

$$u_j^L(\mathbf{x}^L) = \int_{|\mathbf{x}^L|<\delta s} \left[S_{jk}(\mathbf{x}^L,\mathbf{X}^L)\frac{f_k^L(\mathbf{X}^L)}{8\pi\mu} + D_{jk}(\mathbf{x}^L,\mathbf{X}^L)\frac{d_k^L(\mathbf{X}^L)}{4\pi}\right] dX^L, \tag{12}$$

where $\mathbf{f}^L = (f_1^L, f_2^L, f_2^L)$, $\mathbf{d}^L = (-a^2/4\mu)(0, f_2^L, f_3^L)$.

We now assume $\mathbf{f}^L$ to be constant over this short interval and integrate to obtain

$$u_j^L(\mathbf{x}^L) = f_k^L [K_{jk}^L(\mathbf{x}^L - \mathbf{X}^L)]_{\mathbf{X}^L=(-\delta s,0,0)}^{\mathbf{X}^L=(\delta s,0,0)}, \tag{13}$$

where the K_{jk}^L are given by

$$K_{11}^L = \frac{1}{8\pi\mu}\left\{2\ln[r-(x-X)] + \frac{x-X}{r}\right\}, \quad K_{21}^L = \frac{1}{8\pi\mu}\frac{y-Y}{r}, \quad K_{31}^L = \frac{1}{8\pi\mu}\frac{z-Z}{r}, \tag{14a–c}$$

$$K_{12}^L = \frac{1}{8\pi\mu}\left\{\frac{y-Y}{r} - \tfrac{1}{2}a^2\frac{y-Y}{r^3}\right\}, \tag{14d}$$

$$K_{22}^L = \frac{1}{8\pi\mu}\left\{\ln[r-(x-X)] - \frac{(y-Y)^2}{\rho^2}\frac{x-X}{r} - \frac{1}{2}\frac{a^2}{\rho^2}\left[\frac{x-X}{r} + \frac{(y-Y)^2}{\rho^2}\left(\frac{(x-X)^3}{r^3} - 3\frac{(x-X)}{r}\right)\right]\right\}, \tag{14e}$$

$$K_{32}^L = \frac{1}{8\pi\mu}\left\{\frac{(y-Y)(z-Z)}{\rho^2}\left[-\frac{(x-X)}{r} - \frac{1}{2}\frac{a^2}{\rho^2}\left(\frac{(x-X)^3}{r^3} - \frac{3(x-X)}{r}\right)\right]\right\}, \tag{14f}$$

$$K_{13}^L = \frac{1}{8\pi\mu}\left\{\frac{z-Z}{r} - \tfrac{1}{2}a^2\frac{z-Z}{r^3}\right\}, \quad K_{23}^L = K_{32}^L, \tag{14g,h}$$

$$K_{33}^L = \frac{1}{8\pi\mu}\left\{\ln[r-(x-X)] - \frac{(z-Z)^2}{\rho^2}\frac{(x-X)}{r} - \frac{1}{2}\frac{a^2}{\rho^2}\left[\frac{x-X}{r} + \frac{(z-Z)^2}{\rho^2}\left(\frac{(x-X)^3}{r^3} - \frac{3(x-X)}{r}\right)\right]\right\}, \tag{14i}$$

where $$\rho^2 = (y-Y)^2 + (z-Z)^2,$$

all in local co-ordinates.

To see that the velocity is approximately constant around the cross-section, we consider a point on the surface specified by $\mathbf{x}^L = (0, a\cos\theta, a\sin\theta)$ and let $\delta s = q$, where $a \ll q < L$. We substitute the expressions (14) for the K_{jk}^L into (13) to find the velocity at this point. We note that the off-diagonal elements K_{jk}^L have zero contribution, as the point chosen is at the centre of the interval of integration. Thus we find that to order a^2/q^2 the velocity of a point on the surface is

$$\mathbf{u}^L = \left(\frac{f_1^L}{2\pi\mu}\left[\ln\frac{2q}{a} - \tfrac{1}{2}\right], \frac{f_2^L}{4\pi\mu}\left[\ln\frac{2q}{a} + \tfrac{1}{2}\right], \frac{f_3^L}{4\pi\mu}\left[\ln\frac{2q}{a} + \tfrac{1}{2}\right]\right). \tag{15}$$

We note that this expression is independent of θ, and hence that the velocity is constant around the cross-section.

This analysis shows that the variation in $\mathbf{u}^L$ around the cross-section due to singularities within a distance q is $O(a^2/q^2)$. On the other hand, the definition (1) of the Stokeslet ensures that the variation due to singularities further distant than q is also $O(a^2/q^2)$. This presentation of slender-body theory is essentially similar to the discussion given by Lighthill (1976, pp. 194–196). In the same paper, he demonstrates that the errors due to centre-line curvature and variation in $\mathbf{f}^L$ in the above expression (15) are $O(\kappa a)$ and $O(\xi a)$ respectively. Here κ is the curvature and ξ is $(f^L)^{-1}df^L/dX^L$.

The analysis above is valid far from the ends of the flagellum. Tuck (1964) considered the effects of blunt ends. Although the error in $\mathbf{f}^L$ at the end may be of order

unity, the integrated effect on the rest of the body is at worst $O(a/L)$. This result holds at the free end, but at the end attached to the cell body, we must consider the effect of the images.

We wish to show that the velocity induced by the image singularities does not vary around the cross-section of the flagellum. Since the images are confined within the sphere, we need consider only the length of the flagellum within a distance q of the surface. The flagellum is attached to the sphere radially, hence the Stokeslets near the surface of the sphere ($|\mathbf{X}| < A+q$) are at points $(A+\epsilon, 0, 0)$. To first order, the images of these singularities are Stokeslets of the same magnitude, but opposite sign, at the points $(A-\epsilon, 0, 0)$. As the Stokeslets and their images are the same distance from the surface of the sphere, it follows that the variation in the induced velocity around the cross-section is of the same order as that at the free end. Stokeslets a distance q or greater from the surface ($|\mathbf{X}| > A+q$) will induce images a distance q or greater from the surface in the interior of the sphere. From the definition of a Stokeslet, it follows that the variation in the velocity induced by these singularities is of order $(a/q)^2$.

Finally, we must show that the velocity due to the rotation of the cross-section is negligible. The angular velocity due to the wave motion is linearly proportional to the curvature and the wave speed. Therefore the velocity on the surface due to the rotation of the cross-section is $O(\kappa a)$ in comparison with the translational velocity. In addition, we need to consider the effect of the rotlet strength on the moment balance for the organism. For the axes perpendicular to the direction of wave propagation, the contribution of the rotlets to the moment balance is $O(a^2/L^2)$. For two-dimensional waves the moment about the axis parallel to the wave direction is identically zero, while for three-dimensional waves it is $O(a^2/A^2)$. This is negligible, as we have assumed $a \ll A$.

4. Integration of singularity distributions

Having demonstrated the validity of slender-body theory and the image system in the solution of this problem, we now turn our attention to finding the induced velocity, which is obtained by integrating the singularities. Before proceeding with the integration, we must specify the shape of the flagellum, as it determines the path of the integration.

Choose a co-ordinate system with the origin at the centre of the sphere and the X axis parallel to a line through the nodal points of the travelling wave. (See figure 1.) We call this the body frame. At a particular instant, the centre-line of the flagellum forms a curve in space specified by $\mathbf{X}(s)$, where s is the arc length measured from the point where the flagellum meets the sphere. The unit tangent vector $\mathbf{T}(s)$ is defined by

$$\mathbf{T}(s) = (dX/ds, dY/ds, dZ/ds). \tag{16}$$

The unit normal and binormal vectors are defined by

$$\mathbf{N}(s) = \frac{d\mathbf{T}}{ds}\Big/\left|\frac{d\mathbf{T}}{ds}\right|, \quad \mathbf{B}(s) = \mathbf{T}\times\mathbf{N}. \tag{17}$$

It is convenient to definite the rotation tensor Θ_{jk} as

$$\Theta_{1k}(s) = T_k(s), \quad \Theta_{2k}(s) = N_k(s), \quad \Theta_{3k}(s) = B_k(s). \tag{18}$$

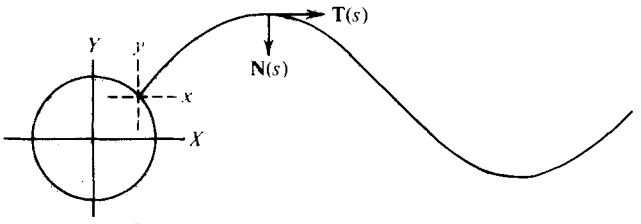

$$s = \int_0^x [1 + \alpha^2 k^2 \cos^2(kx + \phi)]^{\frac{1}{2}}\, dx, \quad y(s) = \alpha \sin[k x(s) + \phi]$$

$$\mathbf{T}(s) = (1, \alpha k \cos[k x(s) + \phi], 0)/(1 + \alpha^2 k^2 \cos^2[k x(s) + \phi])^{\frac{1}{2}}$$

$$\mathbf{N}(s) = (\alpha k \cos[k x(s) + \phi], -1, 0)/(1 + \alpha^2 k^2 \cos^2[k x(s) + \phi])^{\frac{1}{2}}$$

$$\mathbf{B}(s) = (0, 0, -1)$$

$$X(s) = x(s) + A T_1(0), \quad Y(s) = y(s) + A T_2(0) - y(0), \quad Z(s) = 0$$

FIGURE 1. Specification of the sinusoidal wave form showing the co-ordinate system attached to the body. The arrows show the direction of the tangential and normal vectors.

With these preliminaries completed, we now consider the integration of the singularity distributions. We recall from § 3 that the induced velocity is given by the integral of the Stokeslets and dipoles along the flagellum; see (12). The integral obtained does not include the velocity induced by the image singularities inside the sphere. To include these terms, we replace the free-space Green's function S_{jk} in (12) with the Green's function G_{jk} for the flow external to a sphere defined by (3). With this substitution, the expression for the velocity induced by the singularities along the flagellum and their images in the sphere is

$$u_j(\mathbf{x}) = \int_0^L \left[G_{jk}(\mathbf{x}, \mathbf{X}(s)) \frac{f_k(s)}{8\pi\mu} + D_{jk}(\mathbf{x}, \mathbf{X}(s)) \frac{d_k(s)}{4\pi} \right] ds, \tag{19}$$

where the integration extends along the centre-line of the flagellum and all co-ordinates are referred to the body frame.

To evaluate the integral, the flagellum is split into N intervals of length $2\delta s_n$ which are assumed to be straight and along which $\mathbf{f}$ and hence $\mathbf{d}$ are taken as constant. With these assumptions, the integral (19) may be written as

$$u_j(\mathbf{x}) = \sum_{n=1}^{N} \left\{ \frac{f_k(s_n)}{8\pi\mu} \int_{s_n - \delta s_n}^{s_n + \delta s_n} G_{jk}(\mathbf{x}, \mathbf{X}(s))\, ds + \frac{d_k(s_n)}{4\pi} \int_{s_n - \delta s_n}^{s_n + \delta s_n} D_{jk}(\mathbf{x}, \mathbf{X}(s))\, ds \right\}, \tag{20}$$

where

$$s_n = \delta s_n + 2 \sum_{i=1}^{n-1} \delta s_i. \tag{21}$$

We now divide the Green's function G_{jk} into two parts:

$$G_{jk}(\mathbf{x}, \mathbf{X}) = S_{jk}(\mathbf{x}, \mathbf{X}) + S^*_{jk}(\mathbf{x}, \mathbf{X}). \tag{22}$$

Here S_{jk} is the Stokeslet singularity defined by (1) and S^*_{jk} represents the images of the Stokeslet in the sphere. S^*_{jk} is singular inside the sphere, but regular along the flagellum. This makes it possible to evaluate the integral of S^*_{jk} along the flagellum by a simple numerical quadrature. In practice, a simple two- or three-point quadrature is sufficient for each segment. Thus we define

$$H_{jk}(\mathbf{x}, \mathbf{X}(s_n)) = \frac{1}{8\pi\mu} \int_{s_n - \delta s_n}^{s_n + \delta s_n} S^*_{jk}(\mathbf{x}, \mathbf{X}(s))\, ds \tag{23}$$

with the stipulation that the integral is to be evaluated numerically. Substituting this result in (20) gives the induced velocity in the form

$$u_j(\mathbf{x}) = \sum_{n=1}^{N} \left\{ \frac{f_k(s_n)}{8\pi\mu} \int_{s_n-\delta s_n}^{s_n+\delta s_n} S_{jk}(\mathbf{x}, \mathbf{X}(s))\, ds + \frac{d_k(s_n)}{4\pi} \int_{s_n-\delta s_n}^{s_n+\delta s_n} D_{jk}(\mathbf{x}, \mathbf{X}(s))\, ds \right\} + \sum_{n=1}^{N} H_{jk}(\mathbf{x}, \mathbf{X}(s_n)) f_k(s_n). \quad (24)$$

The remaining integrals are recognized as those appearing in (12). To evaluate them, it is necessary only to convert from the local co-ordinate system used in (12) to the general co-ordinates defined in the body frame. The local co-ordinate system for each interval has its origin at the point $\mathbf{X}(s_n)$. The X^L axis is parallel to $\mathbf{T}(s_n)$ and the Y^L and Z^L axes are parallel to $\mathbf{N}(s_n)$ and $\mathbf{B}(s_n)$ respectively. In general co-ordinates, the local point $\mathbf{x}^L$ is expressed by

$$x_j^L = \Theta_{jk}(s_n)\,[x_k - X_k(s_n)]. \quad (25)$$

Using this definition and the rule for transforming tensors, we can write (13) in general co-ordinates; hence the velocity induced by the singularities in the nth interval is

$$u_j(\mathbf{x};\, s_n) = K_{jk}(\mathbf{x}, \mathbf{X}(s_n)) f_k(s_n), \quad (26)$$

where
$$K_{jk}(\mathbf{x}, \mathbf{X}(s_n)) = \Theta_{ij}(s_n)\, \Theta_{lk}(s_n)\, [K_{il}^L(\mathbf{x}^L - \mathbf{X}^L)]_{\mathbf{X}^L=(-\delta s_n,\,0,\,0)}^{\mathbf{X}^L=(\delta s_n,\,0,\,0)}. \quad (27)$$

Substituting this result into (24), we find that the velocity induced by the distributed singularities is

$$u_j(\mathbf{x}) = \sum_{n=1}^{N} \{[K_{jk}(\mathbf{x}, \mathbf{X}(s_n)) + H_{jk}(\mathbf{x}, \mathbf{X}(s_n))] f_k(s_n)\}. \quad (28)$$

5. Kinematics of flagellar motions

We now turn our attention to specification of the shape of the flagellum as a function of time and the determination of the velocity of points along the flagellum. In the previous section, the shape of the flagellum at a particular instant was specified by $\mathbf{X}(s)$. We generalize this representation to consider a function $\mathbf{X}(s,t)$, where s is as defined before and $\mathbf{X}(s,t)$ is referred to the body frame. For an inextensible flagellum, the velocity with respect to the body frame of a point at the position s is

$$\mathbf{u}(s,t) = \partial \mathbf{X}(s,t)/\partial t. \quad (29)$$

This expression is valid for any type of motion; however, we are primarily interested in transverse waves propagating along the flagellum. In a frame moving with the wave, the shape of the flagellum is specified by $\mathbf{X}^w(s-ct)$, where c is the arcwise wave speed. The wave is assumed to have arcwise wavelength Λ and linear wavelength λ, hence

$$X^w(s+\Lambda) = X^w(s) + \lambda, \quad Y^w(s+\Lambda) = Y^w(s), \quad Z^w(s+\Lambda) = Z^w(s). \quad (30)$$

In addition, we note that the wave frame translates, but does not rotate with respect to the body frame. Thus the tangential and normal vectors are identical in the two frames and may be written as $\mathbf{T}(s-ct)$, $\mathbf{N}(s-ct)$ and $\mathbf{B}(s-ct)$.

The velocity of a point with respect to the wave frame is

$$\mathbf{u}^w(s,t) = \partial \mathbf{X}^w(s-ct)/\partial t = -c\, \partial \mathbf{X}^w/\partial s = -c\mathbf{T}(s-ct). \quad (31)$$

To find the velocity with respect to the body frame, we must find the translational velocity of the wave frame with respect to the body frame. To do this, we calculate the velocity of the end point $s = 0$ in each frame.

In the body frame, the point $s = 0$ is at the position $A\mathbf{T}|_{s=0}$. This follows from the condition that the flagellum is attached to the sphere radially. The velocity of this point in the body frame is $-Ac[d\mathbf{T}/ds]_{s=0}$. We note that the point is on the surface of the sphere, from which it follows that the sphere must rotate with respect to the body frame with angular velocity $-\Omega_H \mathbf{B}|_{s=0}$, where Ω_H is defined by

$$\Omega_H = c\,|d\mathbf{T}/ds|_{s=0}. \tag{32}$$

Using this definition, the velocity of the point $s = 0$ in the body frame is $-A\Omega_H \mathbf{N}|_{s=0}$. The velocity of the point in the wave frame is simply $-c\mathbf{T}|_{s=0}$. Therefore the wave frame translates with respect to the body frame with velocity

$$[c\mathbf{T} - A\Omega_H \mathbf{N}]_{s=0}. \tag{33}$$

We note that the average value of this expression is the linear wave speed V, defined as the speed of the wave in a frame in which the particles have no forward displacement. This wave speed is related to the arcwise wave speed c by the equation

$$c/\Lambda = V/\lambda. \tag{34}$$

See Lighthill (1975, pp. 53–54).

Finally, we combine (31) and (33) to obtain the velocity of a point on the flagellum relative to the body frame:

$$\mathbf{u}(s,t) = [c\mathbf{T} - A\Omega_H \mathbf{N}]_{s=0} - c\mathbf{T}(s-ct). \tag{35}$$

6. Boundary conditions

The velocities calculated in the section on flagellar kinematics are expressed relative to the body frame. To find the velocity of each point relative to the fluid, we must consider the translation and rotation of this frame with respect to the fluid at rest at infinity.

We assume that the body frame translates and rotates relative to the fluid at rest with velocity $\mathbf{U}_0$ and angular velocity Ω_0. Therefore the velocity of a point on the flagellum relative to the fluid is

$$\mathbf{u}_R = \mathbf{U}_0 + \Omega_0 \times \mathbf{X} + [c\mathbf{T} - A\Omega_H \mathbf{N}]_{s=0} - c\mathbf{T}. \tag{36}$$

This is the velocity which must be matched by the velocity induced by the flow singularities. These include the Stokeslets and dipoles along the flagellum, together with their images in the sphere. To these we must now add the singularities needed to match the velocity of translation and rotation on the surface of the sphere.

The origin of the body frame is fixed at the centre of the sphere, hence the velocity of the sphere is $\mathbf{U}_0$. The sphere rotates with angular velocity $-\Omega_H \mathbf{B}|_{s=0}$ relative to the body frame, hence it has angular velocity $\Omega_0 - \Omega_H \mathbf{B}|_{s=0}$ relative to the fluid at rest. These velocities are matched by a combination of a Stokeslet, dipole and rotlet. The velocity field generated by these singularities is

$$u_{Hj}(\mathbf{x}) = \tfrac{3}{4}A\left(S_{jk} - \frac{A^2}{3}D_{jk}\right)U_{0k} + \frac{A^3 \epsilon_{jkl} x_l}{|\mathbf{x}|^3}(\Omega_{0k} - \Omega_H B_k|_{s=0}). \tag{37}$$

(See Happel & Brenner 1965, pp. 163, 169.)

The boundary condition on the surface of the organism is that the velocity of each point on the surface must equal the velocity of the fluid at that point. This condition has been satisfied implicitly on the surface of the sphere by our choice of singularities. We have calculated the velocity of each point on the flagellum and the velocity induced by the singularities. Thus the boundary condition on the surface of the flagellum is expressed by

$$u_{Rj} = u_{Hj} + \sum_{n=1}^{N} [K_{jk}(\mathbf{x}, \mathbf{X}(s_n)) + H_{jk}(\mathbf{x}, \mathbf{X}(s_n))] f_k(s_n), \tag{38}$$

where $\mathbf{u}_R$ is given by (36) and $\mathbf{u}_H$ is given by (37). This expression has $3N + 6$ unknowns: $f_k(s_n)$, $\mathbf{U}_0$ and $\boldsymbol{\Omega}_0$. We evaluate (38) at the N points $\mathbf{X}(s_m)$ to obtain $3N$ equations. The six additional equations are obtained from the force and moment balances.

7. Force and moment balances

The organism is self-propelled and is not influenced by any external forces. Therefore we require that the total force and moment on the organism equal zero. As a Stokeslet corresponds to a point force, the condition of zero force is equivalent to the total Stokeslet strength being zero. To find the total Stokeslet strength, we must consider the Stokeslets along the flagellum, their images inside the sphere and the Stokeslet due to translation of the sphere. The Stokeslet due to translation of the sphere has strength $6\pi\mu A\mathbf{U}_0$. To find the strength of the images inside the sphere, we must consider the radial and transverse components of the Stokeslets along the flagellum.

Let $\mathbf{F}$ be a Stokeslet along the flagellum. We write F_k in the form

$$F_k = \left(F_j \frac{X_j X_k}{X_l X_l}\right) + \left(F_k - F_j \frac{X_j X_k}{X_l X_l}\right), \tag{39}$$

where the first bracket contains the radial component and the second the transverse component with respect to the sphere.

Equations (7) and (8) give the strength of the radial image and transverse image respectively. Adding these image strengths, we find that the total force on the organism due to a Stokeslet and its image is

$$F_k(1 + C_T) + F_j \left(\frac{X_j X_k}{X_l X_l}\right)(C_R - C_T), \tag{40}$$

where

$$C_R = -\frac{3}{2}\frac{A}{|\mathbf{X}|} + \frac{1}{2}\frac{A^3}{|\mathbf{X}|^3}, \quad C_T = -\frac{3}{4}\frac{A}{|\mathbf{X}|} - \frac{1}{4}\frac{A^3}{|\mathbf{X}|^3}. \tag{41}$$

Summing over all Stokeslets on the flagellum and adding the contribution due to the translation of the sphere, the force balance becomes

$$\sum_{n=1}^{N} \left[f_k(s_n)(1 + C_T(s_n)) + f_j(s_n)\frac{X_j X_k}{X_l X_l}(C_R(s_n) - C_T(s_n))\right] 2\delta s_n + 6\pi\mu A U_{0k} = 0. \tag{42}$$

For the moment balance, we need consider only the transverse component of $\mathbf{F}$, as the radial component has zero moment about the centre of the sphere. The strength of the image rotlet for the transverse component is given by (8). The moment about the centre of the sphere due to a Stokeslet $\mathbf{F}$ at the point $\mathbf{X}$ and its images is

$$\epsilon_{ijk} X_j F_k (1 - A^3/|\mathbf{X}|^3). \tag{43}$$

The moment about the origin due to the rotation of the sphere is

$$8\pi\mu A^3(\boldsymbol{\Omega}_0 - \Omega_H \mathbf{B}|_{s=0}). \tag{44}$$

Therefore the moment balance gives

$$\sum_{n=1}^{N} \left[\epsilon_{ijk} X_j f_k(s_n)\left(1 - \frac{A^3}{|\mathbf{X}|^3}\right)\right] 2\delta s_n + 8\pi\mu A^3(\Omega_{0i} - \Omega_H B_i|_{s=0}) = 0. \tag{45}$$

The $3N+6$ system of equations in $3N+6$ unknowns is now complete. It consists of the boundary condition (38) together with the force and moment balances (42) and (45). The $3N+6$ unknowns are $\mathbf{f}(s_n)$, $\mathbf{U}_0$ and $\boldsymbol{\Omega}_0$.

8. Solution of equations

To solve the $3N+6$ system of equations we adopt an iteration procedure. First, we write (38) in a different form by making the following definitions:

$$Q_{jk}(s_m, s_n) = K_{jk}(\mathbf{X}(s_m), \mathbf{X}(s_n)) + H_{jk}(\mathbf{X}(s_m), \mathbf{X}(s_n)), \tag{46}$$

$$P_{jk}(s_m) = \sum_{n=1}^{N} Q_{jk}(s_m, s_n). \tag{47}$$

Thus (38) becomes

$$u_{Rj}(s_m) = u_{Hj}(s_m) + P_{jk}(s_m) f_k(s_m) + \sum_{n=1}^{N} [f_k(s_n) - f_k(s_m)]\, Q_{jk}(s_m, s_n). \tag{48}$$

We then multiply by the inverse of P_{jk} and rearrange the terms to obtain

$$f_i(s_m) = P_{ij}^{-1}(s_m)\left\{u_{Rj}(s_m) - u_{Hj}(s_m) - \sum_{n=1}^{N} [f_k(s_n) - f_k(s_m)]\, Q_{jk}(s_m, s_n)\right\}. \tag{49}$$

We use this expression to define the iteration. The right-hand side of the equation depends on the previous values of $\mathbf{f}$ and $\mathbf{U}_0$ and $\boldsymbol{\Omega}_0$, while the left-hand side defines the next iterated value for $\mathbf{f}$. The advantage of the iteration method is that it does not require the inversion of a $3N \times 3N$ matrix. To find $\mathbf{U}_0$ and $\boldsymbol{\Omega}_0$ at each iteration, we might define an iterate similar to that for $\mathbf{f}$, but this is not the best way to proceed. Alternatively, we might make use of the linearity of the equations and find an iterative solution for each component of $\mathbf{U}_0$ and $\boldsymbol{\Omega}_0$ independently. This technique leads to great simplification when attempting a solution through the use of perturbation methods but is inefficient for numerical solutions. To find the complete solution as efficiently as possible, we use (49) to eliminate $\mathbf{f}$ from (42) and (45) at each iteration. The six equations for $\mathbf{U}_0$ and $\boldsymbol{\Omega}_0$ are then solved simultaneously.

The advantage of this method is that the complete solution for $\mathbf{f}$ and all components of $\mathbf{U}_0$ and $\boldsymbol{\Omega}_0$ is obtained in the same step. In addition, the iteration converges more rapidly than if $\mathbf{U}_0$ and $\boldsymbol{\Omega}_0$ are iterated in the same manner as $\mathbf{f}$. Finally, the solution of one 6×6 system and N 3×3 systems requires far less computer time and storage than the direct inversion of the $(3N+6)$-order matrix.

The solution obtained for the system of equations is the solution at only one instant of time. To find the average value for $\mathbf{U}_0$ and $\boldsymbol{\Omega}_0$, we must find the solution of the equations at several points in the cycle. We define the average swimming speed as the displacement of the sphere in a cycle divided by the period of the cycle. This is not the

simple average of $\mathbf{U}_0$ because it is measured in a frame which rotates with angular velocity $\boldsymbol{\Omega}_0$. We define the rotation tensor Φ_{jk} such that

$$X_{Rj} = \Phi_{jk}(t)\, X_k, \tag{50}$$

where $\mathbf{X}$ is a vector referred to the body frame and $\mathbf{X}_R$ is referred to the frame at rest with respect to the fluid. We cannot write down an explicit expression for Φ_{jk}, but we have the following relationship from the definition of $\boldsymbol{\Omega}_0$:

$$d\Phi_{jk}(t)/dt = \epsilon_{klm}\, \Phi_{jl}\, \Omega_{0m}, \tag{51}$$

with initial condition $\Phi_{jk} = \delta_{jk}$ at $t = 0$. With this definition, we have as the average swimming speed

$$\bar{U}_j = \frac{1}{\tau}\int_0^\tau \Phi_{jk}(t)\, U_{0k}(t)\, dt. \tag{52}$$

To evaluate this expression, we solve the equations at M points in the cycle and fit an M-term Fourier series for $\mathbf{U}_0(t)$ and $\boldsymbol{\Omega}_0(t)$. The Fourier series give continuous functions of time for $\mathbf{U}_0(t)$ and $\boldsymbol{\Omega}_0(t)$. These functions are used to integrate (51) and (52) to find the average swimming speed. The integral of (52) over sub-intervals gives the trajectory of the organism.

In addition to the swimming speed, we are interested in the average power consumption of the organism. We can write the instantaneous power consumption as the integral of $\mathbf{F}.\mathbf{U}_R$ over the surface of the organism, where $\mathbf{F}$ is the force per unit area and $\mathbf{U}_R$ is the velocity relative to the rest frame. This calculation requires the surface distribution of force on the sphere. To overcome this difficulty, we use the fact that the total force and moment on the organism are zero. This allows us to calculate the power with $\mathbf{U}$ referred to any frame. Accordingly, we choose the frame in which the sphere has zero velocity and angular velocity. The integral is then restricted to the flagellum, and we use the force per unit length $\mathbf{f}$. Thus the instantaneous power is

$$P(t) = \sum_{n=1}^{N} f_k(s_n)\, U_k(s_n)\, 2\delta s_n, \tag{53}$$

where

$$\mathbf{U}(s_n) = [c\mathbf{T} - A\Omega_H \mathbf{N}]_{s=0} - c\mathbf{T}(s_n) - \Omega_H \mathbf{B}|_{s=0} \times \mathbf{X}(s_n). \tag{54}$$

The average power consumption is

$$\bar{P} = \frac{1}{\tau}\int_0^\tau P(t)\, dt, \tag{55}$$

and as before, we evaluate $P(t)$ at M points in the cycle and evaluate the integral numerically.

9. Results

We have developed a method for analysing the locomotion of micro-organisms by flagellar motions. In applying this method, we wish to examine a wide variety of organisms to determine the effects of changes in the various parameters, and how biological considerations affect their values. It is impossible to examine all combinations of wave form and body dimensions, hence we must restrict our attention to a

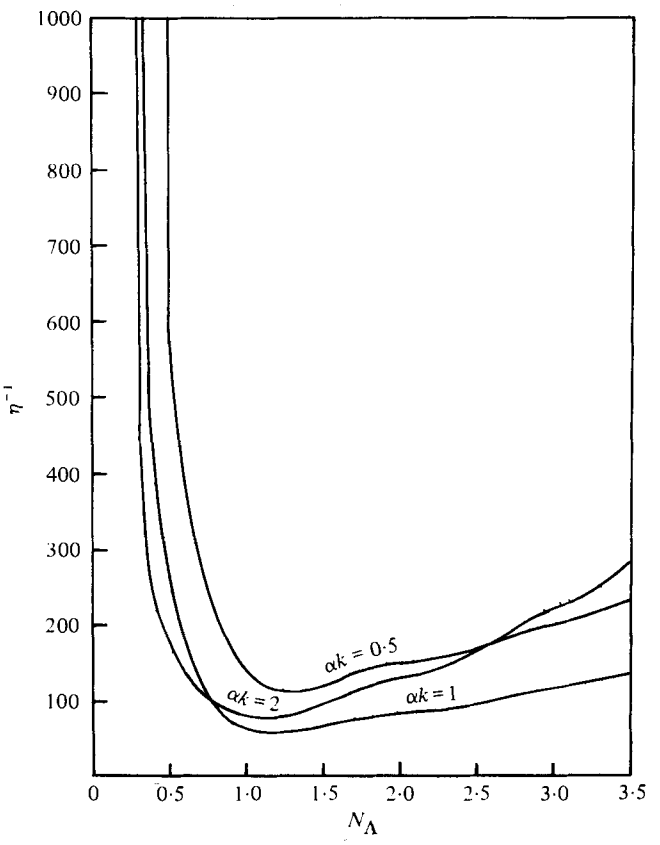

FIGURE 2. Power consumption in the non-dimensional form (56) as a function of number of wavelengths N_Λ, for a slender organism without a cell body. Curves are for different amplitudes αk, with $a/L = 0{\cdot}01$.

more limited class. In this paper, we consider organisms employing planar sinusoidal waves. We indicate in each circumstance whether the result holds for more general planar wave forms or is unique to this wave form. We note that many organisms actually employ sinusoidal waves, particularly the spermatozoa of several species.

The organisms we consider have cell body radius A, flagellar radius a and flagellar length L. The sinusoidal wave has amplitude α, linear wavelength λ and linear wave speed V. The wavenumber k is equal to $2\pi/\lambda$. The various position vectors are shown in figure 1. We specify the body by the non-dimensional parameters a/L and A/L and the wave by the non-dimensional parameters αk and N_Λ, where N_Λ, the number of waves on the flagellum, equals L/Λ. The average swimming speed is non-dimensionalized as $\overline{U}/V$, where $\overline{U} = |\overline{\mathbf{U}}|$. In considering the power consumption, we use the following non-dimensional form, sometimes called the inverse efficiency:

$$\eta^{-1} = \overline{P}/[(6\pi\mu A + K_T L)\,\overline{U}^2], \tag{56}$$

with

$$K_T = 2\pi\mu/\ln(2L/a). \tag{57}$$

The expression in the denominator of (56) is the approximate power required to pull the organism through the water at its average swimming speed.

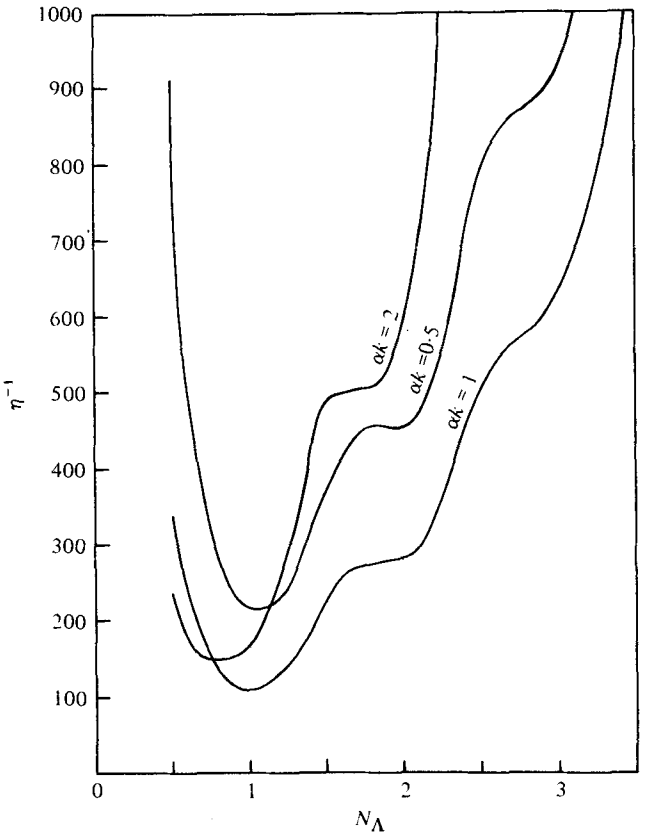

FIGURE 3. Power consumption (56) as a function of number of wavelengths N_Λ for an organism with a large cell body (radius $A/L = 0{\cdot}1$). Curves are for different amplitudes αk, with $a/L = 0{\cdot}01$.

In examining the effects of the parameters on the swimming speed and power consumption, we are interested in determining the optimal swimming motion. This is not necessarily the motion which produces the fastest swimming speed, but rather that which requires the lowest power consumption at a given swimming speed.

It is difficult to show variation with respect to four parameters, but a logical way to proceed is to consider first the wave parameters and then the body parameters. Accordingly we consider the power consumption η^{-1} as a function of the number of waves N_Λ. Figure 2 shows this function for a headless organism at three different wave amplitudes αk. At small values of N_Λ, the organism has a very large power consumption. This is due to the fact that the entire flagellum forms a fraction of the wave, causing excessive yawing motion and little forward progress. This effect decreases as the optimum value $N_\Lambda = 1$ is approached. The slowly increasing behaviour as N_Λ increases from 1 is due to interference between neighbouring crests as they are brought closer together. This explains why the curve for $\alpha k = 2$ rises more quickly than the others. For smaller values of a/L this effect is less pronounced, as the interaction radius is proportionately smaller. Figure 3 shows the behaviour of η^{-1} for the same wave forms but with the flagellum attached to a large cell body. The behaviour is similar, with the optimum at $N_\Lambda = 1$ for $\alpha k = 0{\cdot}5$ and 1 and at $N_\Lambda = 0{\cdot}8$ for $\alpha k = 2$.

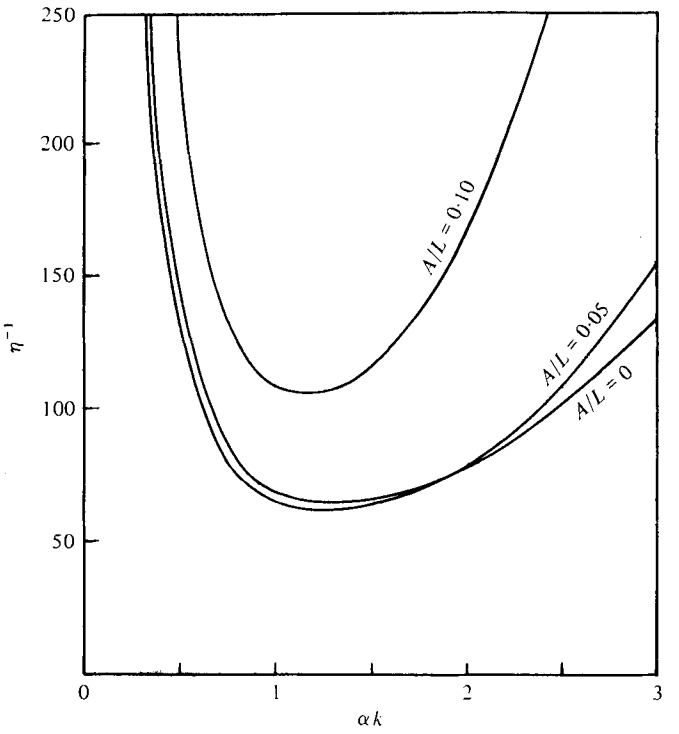

FIGURE 4. Power consumption (56) as a function of amplitude αk. Curves are for organism without a cell body and for two different head radii A. Single wavelength, $N_\Lambda = 1$ ($a/L = 0{\cdot}01$).

The interaction effect is more extreme because the flagellum must generate extra thrust to overcome the drag of the cell body. The large number of inflexions in both figures is due to 'resonances' which occur at various values of N_Λ where there is less yawing motion.

If we compare these results with those for real organisms we find reasonable agreement. For headless organisms, we find that nematodes and other swimming worms have N_Λ in the range 1–2. Among organisms with a cell body, we find that a number, including the sea-urchin spermatozoa studied by Gray & Hancock (1955), have N_Λ in the range 1–1·5. On the other hand, there are numerous organisms employing several waves along their flagella. This discrepancy is due to two factors. The first, which has already been mentioned, is that smaller values of a/L ($\leqslant 0{\cdot}001$) reduce the interaction effect and produce virtually no increase in η^{-1} for large values of N_Λ. The second factor is the use of non-sinusoidal waves, such as those shown by Brokaw (1965), which are of large amplitude but keep sufficient space between neighbouring waves to minimize interaction effects. Finally, we note that virtually no organisms have N_Λ less than 0·75.

As the value $N_\Lambda = 1$ is the optimum or very close to the optimum in each case, we consider only this value in examining the effect of the other parameters. Figure 4 shows the behaviour of η^{-1} as a function of the amplitude αk for three different organisms. The optimum amplitude is in the range $\alpha k = 1$–1·25. The nature of the propulsive wave is such that the segments of the flagellum nearly parallel to the wave direction produce drag, while those inclined at a large angle to the wave direction produce the thrust.

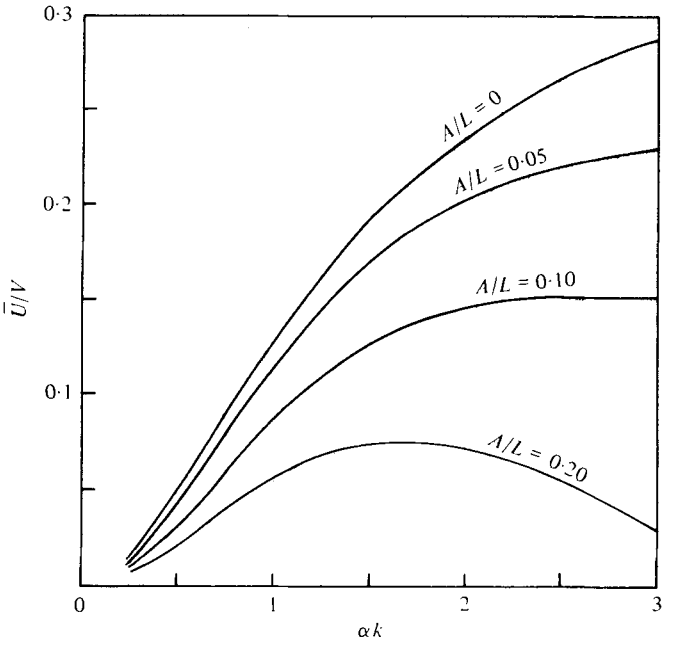

FIGURE 5. Average swimming speed as a function of amplitude αk. Curves are for an organism without a cell body and for three different head radii A. Single wavelength, $N_\Lambda = 1$ ($a/L = 0{\cdot}01$).

This explains the high power consumption at low amplitudes, where the flagellum does not depart far from the wave direction. The increase in η^{-1} for large αk is due to the interference effect as the steepening wave brings the crests closer together. The optimum for an organism with a large cell body is much sharper, because the flagellum must generate extra thrust to overcome the drag of the cell body.

Figure 5 shows the behaviour of $\bar{U}/V$ as a function of αk. For the headless organism and for $A/L = 0{\cdot}05$, the swimming speed rises monotonically with increasing amplitude, levelling off as αk approaches 3. This levelling-off is due to the interference between segments of the flagellum as the increasing amplitude brings them closer together. For the two organisms with large cell bodies, the curves level off at smaller values of αk. In the case $A/L = 0{\cdot}20$, the swimming speed decreases significantly at large amplitudes. The behaviour in these cases is due partly to the interference effect mentioned above, but more important, to the interaction of the flagellum and the cell body. When the wave amplitude and cell body are large enough, the flagellum curves back in the vicinity of the cell body, causing excess drag and reducing the swimming speed. This combination is very inefficient.

In comparing the predicted optimum αk with the values found among actual organisms, we must restrict our attention to those organisms which employ waves nearly sinusoidal in form. This is because the optimum is critically dependent on such factors as the angle the flagellum makes with the wave direction and the separation between waves. These factors are determined as much by the precise form of the wave as by its amplitude and wavelength. With these restrictions, we find good agreement with actual organisms. A wide range of organisms employ waves with αk in the range 1·0–1·5. Typical values for swimming worms such as nematodes are in the range

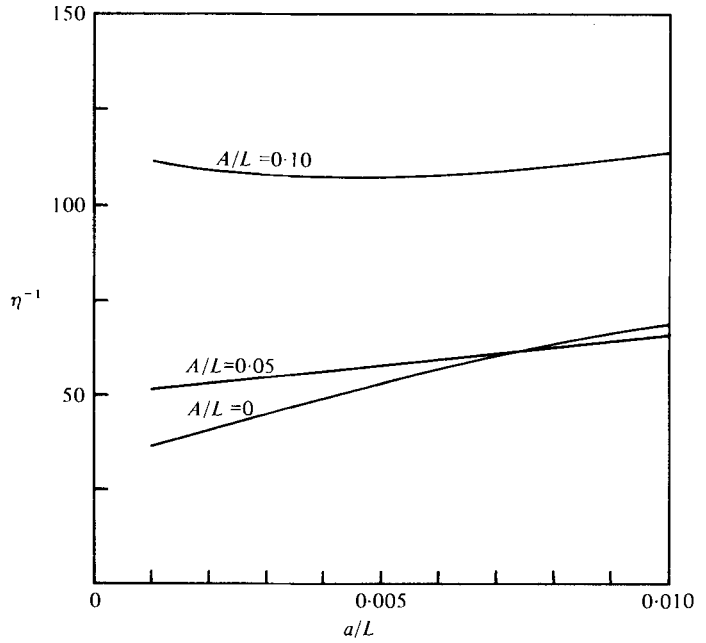

FIGURE 6. Power consumption in the non-dimensional form (56) as a function of flagellar radius a. Curves are for an organism without a cell body and for two different head radii A. (Wave form: $N_\Lambda = 1$, $\alpha k = 1$.)

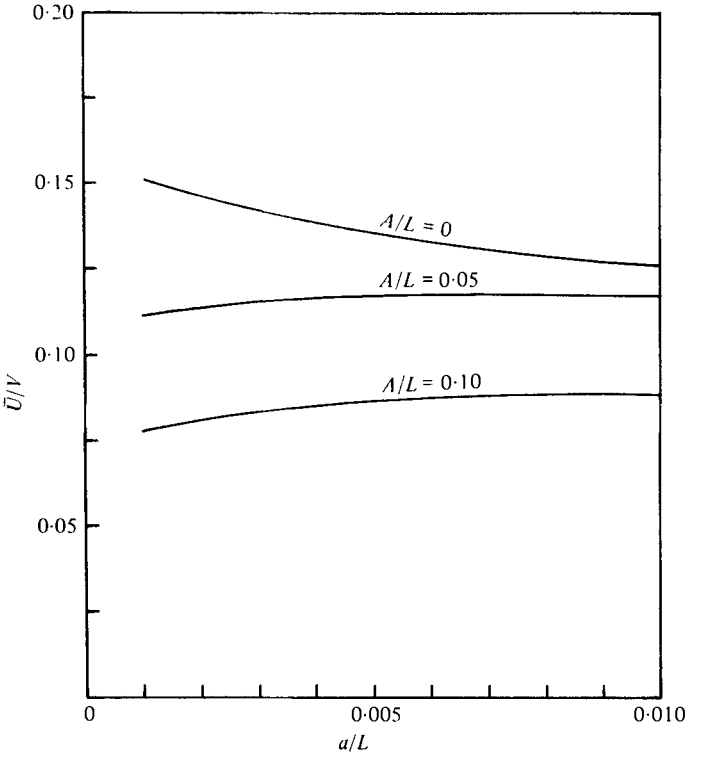

FIGURE 7. Average swimming speed as a function of flagellar radius a. Curves are for an organism without a cell body and for two different head radii A. (Wave form: $N_\Lambda = 1$, $\alpha k = 1$.)

$\alpha k = 0{\cdot}75$–$1{\cdot}0$, while the sea-urchin spermatozoa studied by Gray & Hancock (1955) have αk between 0·8 and 1·2.

From consideration of the results above, we conclude that the optimum sinusoidal wave has N_Λ in the range 0·8–1 and αk in the range 1·0–1·25. The wave with $N_\Lambda = 1$, $\alpha k = 1$ is very close to the optimum for an organism with or without a cell body, hence we shall use these values in considering the effects of variation of the other parameters.

Figure 6 shows the power consumption as a function of a/L. It increases slowly with increasing a/L for a headless organism and varies negligibly for organisms with cell bodies. The mild behaviour in all three cases is due to the logarithmic dependence on a/L observed in slender-body theory. Figure 7 shows the dependence of the swimming speed on a/L. Once again, we observe negligible variation over the range of values considered.

As no optimum flagellar radius is predicted by the theory, we cannot make a comparison with actual organisms. We simply note that all observed values of a/L fall in the range considered here.

Finally, we examine the dependence of power consumption and swimming speed on L/A. In considering the power consumption, we pose the following question: given an organism with specified a and A, what is the optimum value of L? This is the correct way to pose this question, because the head radius and flagellar radius are often constrained by biological considerations, while the flagellar length is free to vary over a wide range. To answer this question, we consider a fixed value of a/A and consider the behaviour of the power consumption as a function L/A. Because L varies in this case, we consider the power consumption in the non-dimensional form

$$\eta_0^{-1} = \overline{P}/6\pi\mu A\,\overline{U}^2. \tag{58}$$

This expression is such that it does not give credit for overcoming the drag of the flagellum, and its minimum will be the most advantageous for the organism. Figure 8 shows the dependence of η_0^{-1} on L/A. We see that the optimum is at $L/A = 25$, and that η_0^{-1} is very close to the optimum over the range $L/A = 20$–40. For values of L/A less than the optimum the flagellum is too short, and the wave motion is inefficient owing to the interference with the cell body. For extremely long flagella, more power is required to overcome the drag of the flagellum than is required for the cell body. Figure 9 shows the swimming speed as it varies with respect to L/A. We see a sharp rise in speed up to $L/A = 25$, and then a rapid levelling-off. This again demonstrates that past a certain point the extra flagellar length does not benefit the organism.

We find that the optimum flagellar length predicted by the theory agrees quite well with the flagellar length of most spermatozoa. On the other hand, protozoa typically have a much shorter flagellum with $L/A = 5$. This discrepancy is due to the fact that the organisms do not use sinusoidal waves. If non-sinusoidal planar waves or three-dimensional waves are used, the interaction of the flagellum and cell body may be quite different, producing a different optimum value for L/A.

Finally, we consider a detailed solution for a single set of parameters. We choose $N_\Lambda = 1$, $\alpha k = 1$, $a/L = 0{\cdot}01$ and $A/L = 0{\cdot}05$. This set of parameters is at or near the optimum for each parameter and is fairly typical of a number of spermatozoa. In figure 10 (*a*), the wave form is shown at one instant in its cycle. Figure 10 (*b*) shows the distribution of thrust per unit length along the flagellum. We clearly see that those

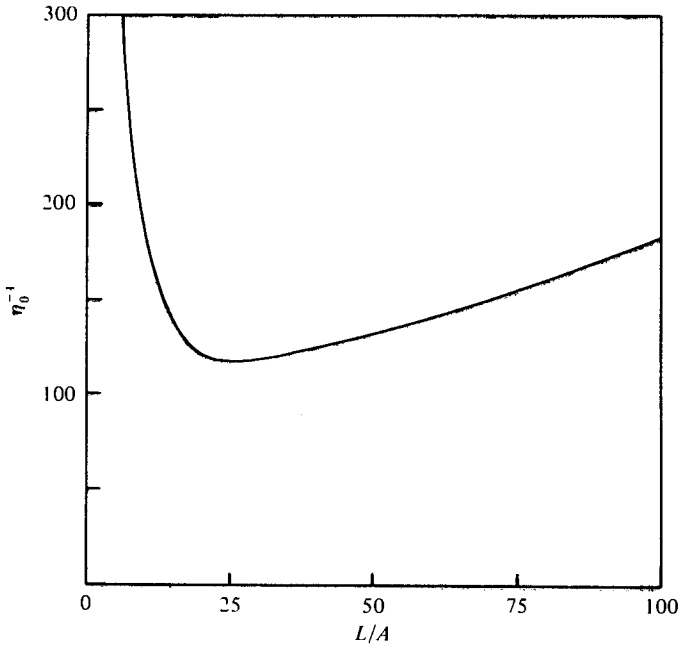

FIGURE 8. Power consumption in the non-dimensional form (58) as a function of flagellar length L. Flagellar radius equal to 0·1 of head radius ($a/A = 0{\cdot}1$). (Wave form: $N_\Lambda = 1$, $\alpha k = 1$.)

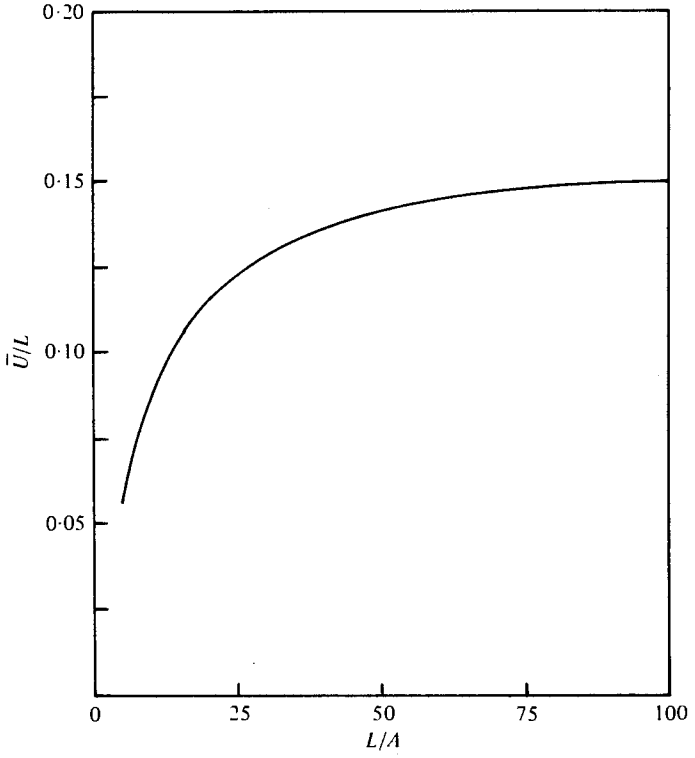

FIGURE 9. Average swimming speed as a function of flagellar length L. Flagellar radius equal to 0·1 of head radius ($a/A = 0{\cdot}1$). (Wave form: $N_\Lambda = 1$, $\alpha k = 1$.)

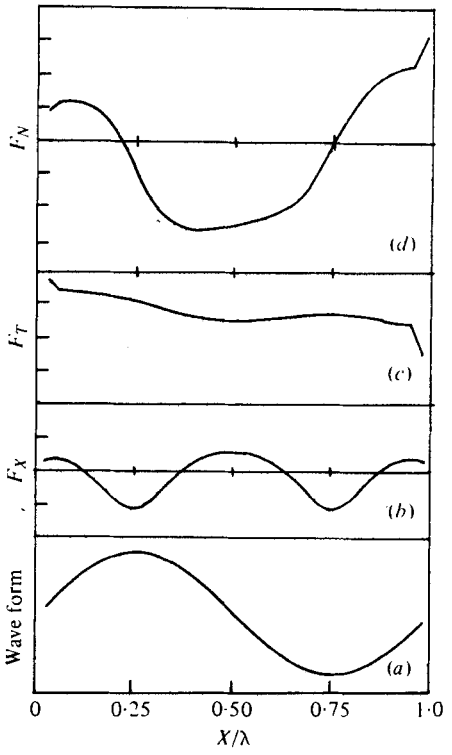

FIGURE 10. (*a*) Typical wave form at one instant of time. (*b*) Thrust per unit length for wave shown; thrust is positive. (*c*) Tangential force per unit length for wave shown. (*d*) Normal force per unit length for wave shown.

segments of the flagellum nearly parallel to the wave direction are producing drag, while those inclined at large angles to the wave direction are producing the thrust.

It is instructive to resolve the force per unit length into its tangential and normal components. These are shown in figures 10(*c*) and (*d*) respectively. We note that the tangential force contributes exclusively to the drag, while the normal force is producing the thrust. Thus it is to the organism's advantage to increase the normal force and decrease the tangential force. In order to generate thrust, the normal force coefficient (the ratio of force per unit length to velocity) must be significantly greater than the tangential force coefficient. In figures 10(*c*) and (*d*) we see that the maximum value of F_N is approximately twice the maximum of F_T. This is as predicted by the asymptotic behaviour of the force coefficients in (15).

Figure 11(*a*) shows the flow field about the organism at the instant of time corresponding to the wave shown in figure 10. The small lines are streaklines, i.e. they are parallel to the velocity at each point and their length is proportional to the magnitude of the velocity. The lines are drawn from points on a rectangular grid, and the length is normalized such that a line of length equal to the grid spacing represents a velocity equal to V.

The streaklines clearly demonstrate the dominance of the normal forces. On the long straight segments of the flagellum at a large angle to the wave direction, the fluid is pushed to the side and slightly to the rear at a speed approximately equal to V. On the

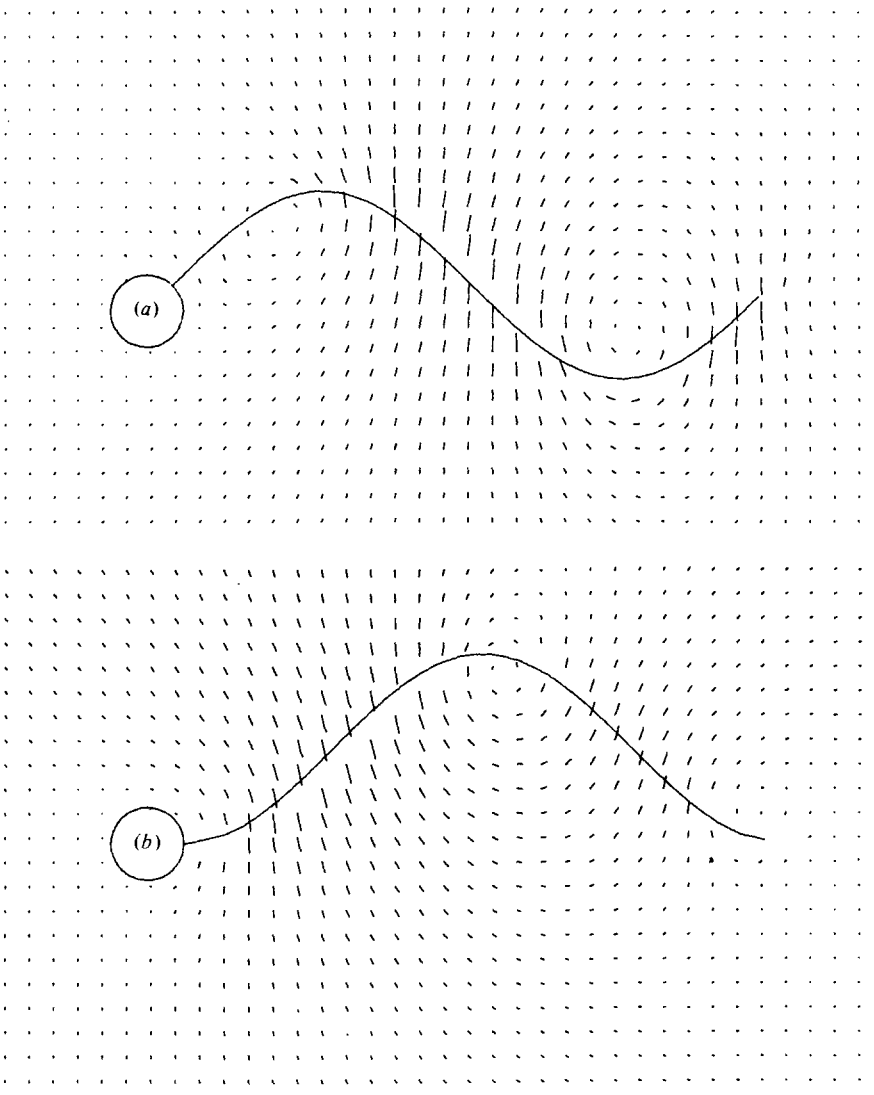

FIGURE 11. (*a*) Streaklines about the organism at one instant during the cycle of the wave. Lines are parallel to the velocity at each point and their length is proportional to the magnitude of velocity. A line of length equal to the grid spacing represents a velocity equal to the linear wave speed V. The wave is travelling to the right. (*b*) Streaklines about the organism one quarter-cycle later.

segments nearly parallel to the wave direction, where the tangential force dominates, the fluid moves forwards along the tangent to the flagellum, but at a much smaller velocity. In the overall picture, we see that the average flow in the wave direction and hence the swimming speed in the opposite direction are very small.

Figure 11 (*b*) shows the pattern of streaklines one quarter-cycle later. At this instant, we see the same dominance of the normal forces, but the overall picture is somewhat different. The average flow in the wave direction is much larger, and the swimming speed is proportionately higher.

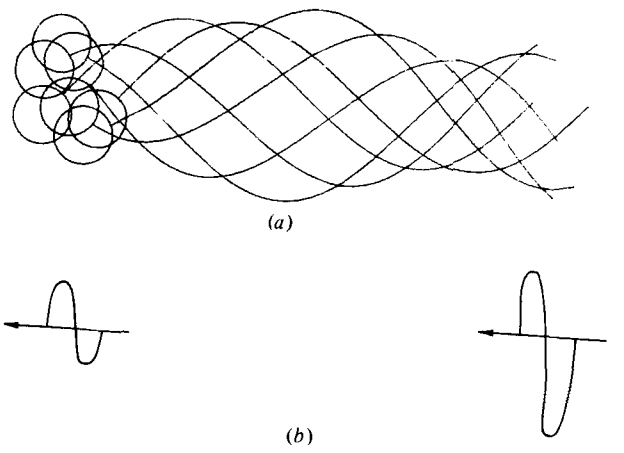

FIGURE 12. (*a*) Trajectory of an organism during one cycle of the wave. (*b*) Trajectory of ends of the flagellum during one cycle of the wave. Arrows indicate swimming direction. Note the apparent increase in amplitude at the trailing end.

The trajectory of the organism during one cycle is shown in figure 12(*a*). The positions of the cell body and flagellum are shown at intervals of one-sixth of a cycle. Figure 12(*b*) shows the trajectory of the end points of the flagellum during the cycle. This figure confirms the non-uniformity in the swimming speed over the cycle inferred from the flow patterns in figure 11. We note that the actual distance travelled is much greater than the distance covered in the swimming direction. An interesting feature of the motion is that the constant amplitude wave appears to have increasing amplitude owing to the yawing motion during the cycle.

We note that for any symmetric wave the organism has zero net rotation over a cycle, and its position at the end of each cycle lies on a line which specifies the swimming direction. The trajectory of the end points of the flagellum is symmetric about a line parallel to the swimming direction.

10. Effectiveness of resistance coefficients

In this section, we consider the use of resistance coefficients to model the swimming of micro-organisms. The initial application of resistance coefficients was by Gray & Hancock (1955), who used coefficients of the form

$$K_T = \frac{2\pi\mu}{\ln(2q/a) - 0{\cdot}5}, \quad K_N = \frac{4\pi\mu}{\ln(2q/a) + 0{\cdot}5}. \tag{59}$$

They reasoned that the value of q was not crucial as the coefficients had only logarithmic dependence on q. They let q equal the wavelength and found that their calculations were very close to observed swimming speeds. Numerous other authors have used these coefficients to calculate the swimming speed and power consumption for a variety of organisms.

Lighthill (1975, p. 52) examined the concept of resistance coefficients from the standpoint of slender-body theory and concluded that q should take a value of approximately one-tenth of the wavelength. Lighthill (1976) calculated an exact

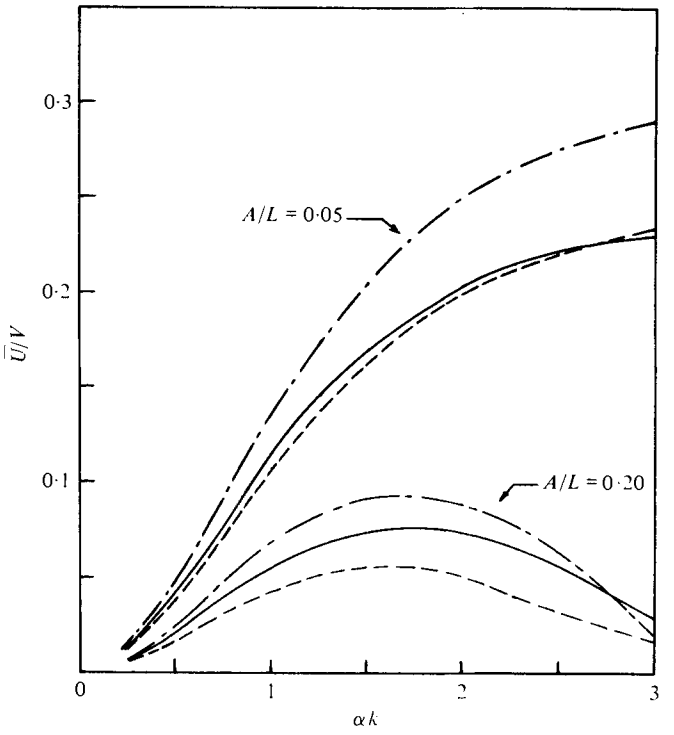

FIGURE 13. Average swimming speed as a function of amplitude αk for two different organisms, showing difference between exact calculation and resistance coefficients. Single wavelength, $N_\Lambda = 1$. Organism dimensions: $a/L = 0{\cdot}01$; $A/L = 0{\cdot}05$, $0{\cdot}20$. ——, exact; – – –, Gray–Hancock; – · –, Lighthill.

solution for an infinite helical wave form. He compared this solution to that obtained using resistance coefficients and concluded that the smaller value of q was appropriate, but that the motion must be considered in two parts. He found that for zero-thrust motion K_N was a good approximation, but that K_T should be of the form

$$K_T = \frac{2\pi\mu}{\ln(2q/a)}. \tag{60}$$

For the extra thrust generated, he proposed a separate coefficient for thrust per unit length. This approach worked quite well for infinite spirals but is rather difficult to apply for finite planar wave forms.

We now compare the results calculated in this paper with those obtained using resistance coefficients. For the calculations using Lighthill's coefficients, only the zero-thrust values are used. Figure 13 shows the swimming speed as a function of αk for two values of A/L. The values $A/L = 0{\cdot}05$ and $0{\cdot}20$ are typical of spermatozoa and protozoa respectively. For the case $A/L = 0{\cdot}05$, we observe that the Gray–Hancock result is very close to the result calculated in this paper. This is to be expected, as the Gray–Hancock coefficients have proved accurate when compared with observed swimming speeds. The result using Lighthill's coefficients is not quite as accurate. This is because they were optimized for an infinite zero-thrust spiral. Thus for organisms with relatively small cell bodies, we find that the Gray–Hancock coefficients provide

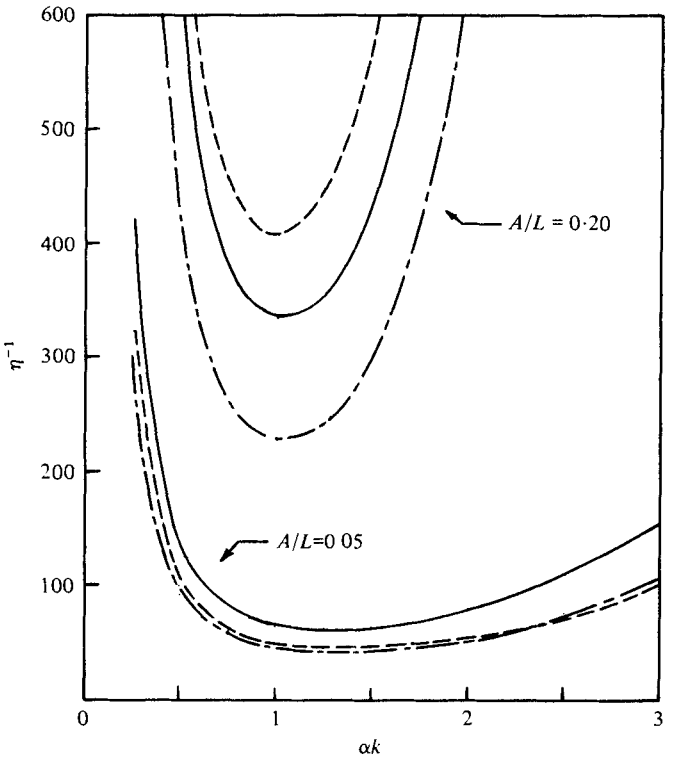

FIGURE 14. Power consumption in the non-dimensional form (56) as a function of amplitude αk for two organisms with different head radii, showing difference between exact calculation and resistance coefficients. Single wavelength, $N_\Lambda = 1$. Organism dimensions: $a/L = 0{\cdot}01$; $A/L = 0{\cdot}05$, $0{\cdot}20$. ——, exact; – – –, Gray–Hancock; – · –, Lighthill.

a good estimate of the swimming speed: accurate to within 10 % over a wide range of the parameters.

For organisms with large cell bodies ($A/L \geqslant 0{\cdot}20$), corresponding to protozoa, we see that neither resistance-coefficient model is very accurate. In general, the error in the swimming speed calculated by resistance coefficients for organisms with large cell bodies is approximately 20 %.

The success of resistance coefficients in predicting the swimming speed for a large number of organisms has given some authors confidence in their use for calculating power consumption. This confidence is not justified, as can be seen in figure 14. In this figure, the power consumption is shown as a function of αk for $A/L = 0{\cdot}05$ and $0{\cdot}2$. For the smaller cell body, both sets of resistance coefficients give values much less than the actual value. In this case, their estimates are approximately the same, but this is not true in general. The error in Lighthill's predictions is due to the overestimate in swimming speed, which causes the power to be underestimated. This is confirmed by the result for the larger cell body. In each case, the Lighthill model underestimates the power by approximately 30 %. The error in the Gray–Hancock estimate is due to two factors. For small cell bodies, the swimming speed is accurate, but the coefficients underestimate the magnitude of the forces, and hence the power consumption, by approximately 30 %. For large cell bodies, the swimming speed is underestimated,

which causes the power to be overestimated. This is offset somewhat by the underestimate of the forces, but still leads to an overestimate of approximately 25 %. For other parameter combinations not shown here, the error with either model reaches 50 %.

In summary, the relative error in the power consumption predicted by resistance coefficients varies from 25 to 50 %. The Lighthill coefficients consistently underestimate the power, while the Gray–Hancock coefficients underestimate the power for small cell bodies and overestimate it for large cell bodies.

From the results above, we conclude that resistance coefficients are unsatisfactory for a complete description of the swimming of micro-organisms. Their values can be optimized for one quantity such as swimming speed, but they cannot give an accurate estimate for power consumption over any range of the parameters. Thus we feel that it is not worthwhile attempting to devise ever 'improved' coefficients when the problem can be solved in a straightforward manner as described here.

11. Conclusions

In this paper, we have presented a method of solving the hydrodynamic equations arising from the swimming motion of a micro-organism with a spherical cell body propelled by a general three-dimensional wave propagating down a long slender flagellum. We have presented results from the numerical solution of the equations for organisms using planar sinusoidal waves, with the object of finding the optimal swimming motion. Resistance-coefficient models have been examined and have proved useful for predicting the swimming speed but unsuitable for providing accurate assessments of the power consumption.

A detailed examination of the results shows the importance of considering the effect on the flow of the entire organism. Models which neglect the presence of the cell body, except in its contribution to the force balance, cannot account for the interaction of the cell body and flagellum, which has an important bearing on the swimming speed and power consumption.

In examining the swimming of micro-organisms, we feel that there are two distinct approaches whose aims are complementary. The first, the one used here, is to examine a wide range of all the parameters with the object of discovering optimal swimming motions and their applicability to actual organisms. The second approach is to consider a single organism and examine the interdependence of the propulsive mechanism and the various biochemical and environmental factors which affect the organism. Although we have not followed this approach in this paper, we wish to emphasize the usefulness of our method of solution in this approach. In particular, the more accurate power estimates are helpful in comparisons with the power available from biochemical sources.

Finally, we emphasize that it is not necessary to restrict the calculations to a sinusoidal wave or to any regular wave form. A major benefit of the numerical solution is that any type of motion may be considered. This includes any form of travelling wave, as well as irregular motions which vary along the flagellum and during the cycle. In a future publication, results will be presented for a variety of three-dimensional motions.

I am indebted to Professor M. J. Lighthill for numerous helpful comments and suggestions. I wish to acknowledge the support of the National Science Foundation through the Graduate Fellowship program.

REFERENCES

BATCHELOR, G. K. 1970 *J. Fluid Mech.* **44**, 419.
BROKAW, C. J. 1965 *J. Exp. Biol.* **43**, 155.
CHWANG, A. T. & WU, T. Y. 1971 *Proc. Roy. Soc.* B **178**, 327.
COAKLEY, C. J. & HOLWILL, M. E. J. 1972 *J. Theor. Biol.* **35**, 525.
COX, R. G. 1970 *J. Fluid Mech.* **44**, 791.
GRAY, J. & HANCOCK, G. J. 1955 *J. Exp. Biol.* **32**, 802.
HANCOCK, G. J. 1953 *Proc. Roy. Soc.* A **217**, 96.
HAPPEL, J. & BRENNER, H. 1965 *Low Reynolds Number Hydrodynamics*. Prentice-Hall.
JOHNSON, R. E. 1977 Ph.D. dissertation, California Institute of Technology.
LIGHTHILL, M. J. 1975 *Mathematical Biofluiddynamics*. Philadelphia: SIAM.
LIGHTHILL, M. J. 1976 *SIAM Rev.* **18**, 161.
MESTRE, N. J. DE & KATZ, D. F. 1974 *J. Fluid Mech.* **64**, 817.
OSEEN, C. W. 1927 *Hydrodynamik*. Leipzig: Akad. Verlag.
SILVESTER, N. R. & HOLWILL, M. E. J. 1972 *J. Theor. Biol.* **35**, 505.
TAYLOR, G. I. 1952 *Proc. Roy. Soc.* A **211**, 225.
TUCK, E. O. 1964 *J. Fluid Mech.* **18**, 619.